PERGAMON

International Journal of Heat and Mass Transfer 45 (2002) 1127–1148

International Journal of HEAT and MASS TRANSFER

www.elsevier.com/locate/ijhmt

Heat transfer by laminar Hartmann flow in thermal entrance region with a step change in wall temperatures: the Graetz problem extended

J. Lahjomri [a], A. Oubarra [a], A. Alemany [b,*]

[a] *Département de Physique, Faculté des Sciences Ain Chok, Université Hassan II, km 8 route El jadida, Maarif B.P. 5366, Casablanca, Morocco*

[b] *Laboratoire des Ecoulements Géophysiques et Industriels, B.P. 53, 38041 Grenoble Cedex 9, France*

Received 22 December 2000; received in revised form 23 February 2001

Abstract

Thermally developing laminar Hartmann flow through a parallel-plate channel, including both viscous dissipation, Joule heating and axial heat conduction with a step change in wall temperatures, has been studied analytically. Expressions for the developing temperature and local Nusselt number in the entrance region are obtained in terms of Peclet number *Pe*, Hartmann number *M*, Brinkman number *Br*, under electrically insulating wall conditions, $\chi = -1$ and perfectly conducting wall conditions, $\chi = 0$. The associated eigenvalue problem is solved by obtaining explicit forms of eigenfunctions and related expansion coefficients. We show that the nonorthogonal eigenfunctions correspond to Mathieu's functions. We propose a new asymptotic solution for the modified Mathieu's differential equation. The asymptotic eigenfunctions for large eigenvalues are also obtained in terms of *Pe* and *M*. Results show that the heat transfer characteristics in the entrance region are strongly influenced by *Pe*, *M*, *Br* and χ.

1. Introduction

The main purpose of this paper is to determine the temperature field and the improved Nusselt number in the thermal entrance region of steady laminar MHD flow through a parallel-plate channel, including viscous dissipation, Joule heating and axial heat conduction with a step change in wall temperatures. This problem corresponds to the study of transverse magnetic field influence on the fundamental extended Graetz problem.

In the absence of magnetic field, it is well known that the extended Graetz problem is defined when axial heat conduction is included in the analysis and its effect becomes important especially at small Peclet number, as in liquid metals for example. The problem has long been in the past and recently the subject of numerous studies, analytical [1–10] and computational [11–16] to generate methods for the extensions of the original Graetz problem without axial heat conduction [17]. In considering the effect of low Peclet number flow on heat transfer, it is often necessary to investigate the problem in two semi-infinite regions of a channel, in upstream ($-\infty < x < 0$) and downstream ($0 < x < +\infty$) regions. The temperature field is then determined in both regions and the two solutions are matched at $x = 0$ where heating (or cooling) starts. Previous studies have clearly shown that this type of problem is related to the determination of a set of eigenvalues and eigenfunctions of a Sturm–Liouville nonselfadjoint operators. The result is such that the eigenfunctions became nonorthogonal and a simple determination of the related expansion coefficients by a classical

* Corresponding author. Tel.: +33-4-7682-5037; fax: +33-4-7682-5271.

E-mail addresses: lahjomri@facsc-achok.ac.ma (J. Lahjomri), oubarra@facsc-achok.ac.ma (A. Oubarra), alemany@hmg.inpg.fr (A. Alemany).

0017-9310/02/$ - see front matter
PII: S0017-9310(01)00205-8

Nomenclature

a	parameter of Mathieu's differential equation, Eq. (24)
A_n, B_n	expansion coefficients
$A^n_{m,4p+n}$	complex expansion coefficients used in Mathieu's solution
b	half-width between parallel-plate channel
$\mathbf{B}_0$	external uniform magnetic field
$Br = PrEc$	Brinkman number, $\mu U_m^2/k(T_0 - T_f)$
$C^n_{m,4p+n}$	complex expansion coefficients used in Mathieu's solution
$\mathrm{ch}(x)$	hyperbolic cosine function
d_0, d_1, d_2, d_3	constants of the fully developed solution
$D(M,\eta)$	dimensionless dissipation function
$E(\varphi,k)$	elliptic integrals of the second kind, $\int_0^{\varphi}[1-k^2\sin^2\alpha]^{1/2}\,\mathrm{d}\alpha$
Ec	Eckert number, $U_m^2/C_p(T_0 - T_f)$
E_z	electric field component
$F(\varphi,k)$	elliptic integrals of the first kind, $\int_0^{\varphi}[1-k^2\sin^2\alpha]^{-1/2}\,\mathrm{d}\alpha$
$f_n, g_n, g_n^0, g_n^1, g_n^{0,1}, h_n$	eigenfunctions
$J_{1/3}$	Bessel function of the first kind
j_z	current density component, Eq. (2)
M	Hartmann number, $B_0 b\sqrt{\sigma/\mu}$
$Nu_{\mathrm{as.}}$	asymptotic Nusselt number
Nu_i	local Nusselt number ($i = 1, 2$), Eq. (18)
Pe	Peclet number, $3U_m b/2\alpha$
Pr	Prandtl number, v/α
q	parameter of Mathieu's differential equation, Eq. (26)
$\mathrm{sh}(x)$	hyperbolic sine function
q_0	parameter, Eq. (24)
T_i	dimensional temperature distribution in the upstream region ($i = 1$) and downstream region ($i = 2$)
T_f	prescribed wall temperature in the downstream region
T_0	prescribed wall temperature in the upstream region
$\mathrm{th}(x)$	hyperbolic tangent function
$u(\eta)$	dimensionless velocity profile, $2/3(u_x(\eta)/U_m)$
U_m	mean fluid velocity of Hartmann flow
$u_x(\eta)$	velocity profile component in the axial direction of Hartmann flow, $U_m((\mathrm{ch}M - \mathrm{ch}M\eta)/(\mathrm{ch}M - (\mathrm{sh}M/M)))$
x	axial coordinate
y	transverse coordinate
z	variable, $M\eta/2$
Greek symbols	
β_n	eigenvalues in the downstream region
$\Gamma(x)$	gamma function
λ_n	eigenvalues in the upstream region
χ	external loading parameter, E_z/B_0U_m
η	dimensionless transverse coordinate, y/b
θ_i	dimensionless temperature distribution, $T_i - T_f/T_0 - T_f$
$\theta_{b,i}$	dimensionless bulk temperature, Eq. (17)
σ	electric conductivity
ξ	dimensionless axial coordinate, x/bPe

method fails. Recently, the present authors [10] have determined the explicit form of the true eigenfunctions and have presented a more efficient procedure for the direct determination of these expansion coefficients for any given fully developed velocity profile.

When the magnetic field is included in the analysis, the influence of this field on the process of heat transfer is globally realized by the modification of the velocity profile and the problem is controlled by the magnitude of three parameters: Peclet number, *Pe*, which characterizes the ratio of axial convection to axial conduction; Hartmann number, *M*, which characterizes the ratio of electromagnetic forces to viscous forces and Brinkman number, *Br*, which represents the ratio of overall dissipation (viscous and Joule heating) to conduction due to the temperature difference at the walls. In this case, we have difficulties similar to those encountered in the case with no applied field (i.e., nonorthogonality of the eigenfunctions and the difficulties in determining both the eigenfunctions and the expansion coefficients). The problem of heat transfer by laminar flow between parallel-plates under the action of transverse magnetic field in two semi-infinite regions, i.e., $-\infty < x < \infty$ was first investigated by Nigam and Singh [18]. These authors used the method of Fourier-sine series and determined only approximately the first three eigenvalues and the corresponding expansion coefficients are calculated by using a variational method. This method yields erroneous results for the important thermal entry region heat transfer. Indeed, the Fourier series representation is extremely slowly convergent in the thermal entrance region and requires a very high number of terms and the resulting equation for eigenvalues involved determinant of infinite order. Consequently, the difficulty of computing the eigenvalues and the determination of corresponding expansion coefficients increased considerably when the order of the determinant becomes larger. Thus, the accuracy of local Nusselt number reported in [18] is therefore questionable. Michiyoshi and Matsumato [19] studied the same problem by neglecting both the effects of viscous dissipation and axial heat conduction under zero net current, open circuit condition. Hwang et al. [20] obtained numerical solutions by implicit difference technique including the effects of viscous and Joule dissipation, nonzero net current and neglecting the axial conduction for the case of prescribed uniform wall heat flux conditions. The problem of MHD channel flow heat transfer with boundary condition of the third kind by neglecting the heat generation was studied by Javeri [21]. The energy equation was solved by applying the Galerkin–Kantorowich method of variational calculus. The temperature evolution in the entrance with semi-infinite region ($0 < x < +\infty$) of an MHD channel by including viscous dissipation, Joule heating, nonzero net current, and axial conduction has been studied by Lecroy and Eraslan [22]. The associated eigenvalue problem was solved by the Galerkin method for the case of constant wall temperature, for constant wall heat flux and with the entrance condition of uniform fluid temperature at $x = 0$. Wu and Cheng [23] studied a similar problem with uniform but unequal wall temperatures in the upper and lower plates with the same entrance boundary condition under open circuit condition. The eigenvalues and the corresponding eigenfunctions were solved by the Runge–Kutta method. However, if one includes both viscous dissipation, Joule heating and axial heat conduction, the entrance condition of uniform fluid temperature at $x = 0$ must be regarded as an approximate one because it is physically unrealistic. In reality, because of the heat conducted upstream, transverse variation in fluid temperature exists in the region $x \leqslant 0$ and the temperature profile at $x = 0$ is greatly affected by axial conduction and heat generation. Consequently, the local Nusselt numbers are different from those obtained by assuming a flat temperature profile at $x = 0$, while the asymptotic Nusselt numbers in the thermally developed region ($x \to +\infty$) for the two problems will be the same and are independent of both Peclet and Brinkman numbers.

It is emphasized that none of the previous studies give any explicit form of the nonorthogonal eigenfunctions and the related expansion coefficients. Furthermore, even for laminar conditions, no precise solution has ever been reported on the values of the local Nusselt number in the important thermal entrance region, precisely in the immediate neighborhood of $x = 0$. The main difficulty in the analysis comes from a singularity which exists for the channel wall temperature at $x = 0$, which in general causes a problem for the numerical modelers. Therefore, an analytical solution near the entrance is required to resolve the singularity.

In this paper, we give the analytical solution of the extended Graetz problem with applied magnetic field taking into account the transverse variation in fluid temperature in the upstream region ($x \leqslant 0$). We show that the nonorthogonal eigenfunctions in upstream and downstream regions correspond to Mathieu's functions. Unlike the previous studies, the eigenfunctions and the corresponding expansion coefficients are obtained in an explicit manner. We propose a new asymptotic solution for modified Mathieu's differential equation for moderate and large values of Hartmann number. This new solution does not exist in the mathematical literature. The asymptotic eigenfunctions for large eigenvalues are also obtained in terms of Hartmann number and with any values of Peclet number. We show that the solution efficiently resolves the singularity. Results show that temperature profiles and local Nusselt number are affected by Peclet, Hartmann, Brinkman numbers and various electrical conditions of the walls.

2. Statement of the problem and mathematical formulation

Consider the extended Graetz problem with prescribed external uniform magnetic field $\mathbf{B}_0$ as shown in Fig. 1. A viscous, incompressible and electrically conducting fluid or liquid metal flows through a long two parallel-plate channel

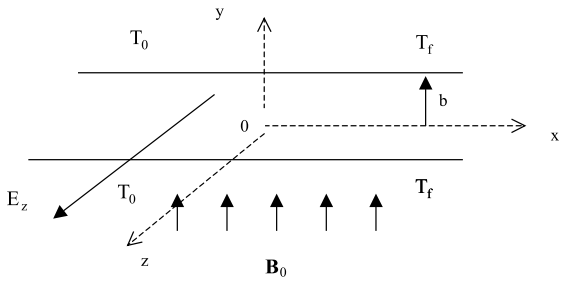

Fig. 1. Problem description.

with laminar regime. We are interested in the part of the channel for which the flow is fully developed. The velocity profile component in the axial direction x for this flow is the well-known Hartmann profile

$$u_x(y) = U_{\mathrm{m}} \frac{(\mathrm{ch}M - \mathrm{ch}M(y/b))}{(\mathrm{ch}M - (\mathrm{sh}M/M))}.$$

The channel walls are maintained at temperature T_0 for $x \leqslant 0$ and T_{f} for $x > 0$. All fluid properties (density ρ, kinematics viscosity v, dynamics viscosity μ, electric conductivity σ, thermal conductivity k, specific heat C_{p}) are assumed to be constant. The free convection caused by the temperature difference is negligible.

2.1. Governing equations

For the hypothesis mentioned above, the energy equation for MHD problem, including viscous dissipation, Joule heating, nonzero net current, governing the field temperature in the semi-infinite upstream and downstream axial regions taking into account the symmetry of the problem with respect to the flow axis is given by

$$\rho C_{\mathrm{p}} u_x(y) \frac{\partial T_i}{\partial x} = k\left[\frac{\partial^2 T_i}{\partial x^2} + \frac{\partial^2 T_i}{\partial y^2}\right] + \mu\left(\frac{\mathrm{d}u_x}{\mathrm{d}y}\right)^2 + \frac{j_z^2}{\sigma} \quad \text{for} \begin{cases} (i = 1, -\infty < x < 0) \\ (i = 2, 0 < x < +\infty) \end{cases} \text{ and } 0 < y < b, \tag{1}$$

where j_z is the electric current density component which can be expressed in terms of $u_x(y)$ and the constant electric field component E_z, and the applied transverse magnetic field $\mathbf{B}_0$ by Ohm's law as:

$$j_z = \sigma[E_z + \mathbf{B}_0 u_x(y)]. \tag{2}$$

Introducing the following dimensionless variables and parameters:

$$\xi = \frac{x}{bPe},$$
$$\eta = \frac{y}{b},$$
$$u(\eta) = \frac{2}{3}\frac{u_x(\eta)}{U_{\mathrm{m}}} = \frac{2}{3}\frac{(\mathrm{ch}M - \mathrm{ch}M\eta)}{(\mathrm{ch}M - (\mathrm{sh}M/M))},$$
$$\theta_i = \frac{T_i - T_{\mathrm{f}}}{T_0 - T_{\mathrm{f}}}.$$

By using Eq. (2), the dimensionless form of the energy Eq. (1) becomes

$$u(\eta)\frac{\partial \theta_i}{\partial \xi} = \frac{\partial^2 \theta_i}{\partial \eta^2} + \frac{1}{Pe^2}\frac{\partial^2 \theta_i}{\partial \xi^2} + BrD(M,\eta) \quad \text{for} \begin{cases} (i = 1, -\infty < \xi < 0) \\ (i = 2, 0 < \xi < +\infty) \end{cases} \text{ and } 0 < \eta < 1, \tag{3}$$

where

$$D(M,\eta) = \frac{M^2 \mathrm{sh}^2 M\eta}{(\mathrm{ch}M - (\mathrm{sh}M/M))^2} + M^2\left[\chi + \frac{\mathrm{ch}M - \mathrm{ch}M\eta}{\mathrm{ch}M - (\mathrm{sh}M/M)}\right]^2$$

is the term due to a viscous dissipation and Joule heating which represents the heat source in the energy equation.

The dimensionless parameters in Eq. (3) are defined as follows:

- $Pe = 3U_m b/2\alpha =$ Peclet number, and $\alpha = k/\rho C_p$ a thermal diffusivity.
- $M = B_0 b\sqrt{\sigma/\mu} =$ Hartmann number.
- $Br = PrEc = \mu U_m^2/k(T_0 - T_f) =$ Brinkman number.
- $Pr =$ Prandtl number, ν/α.
- $Ec =$ Eckert number, $U_m^2/C_p(T_0 - T_f)$.
- $\chi = E_z/B_0 U_m$ is the external loading parameter characterizing various operational modes of the channel; $\chi = -1$ for electrically insulating walls or open circuit condition and $\chi = 0$ for perfectly conducting walls or short circuit condition.

The boundary conditions associated to (3) are well known:

$$\frac{\partial\theta_i}{\partial\eta} = 0 \quad \text{if } \eta = 0 \ \forall -\infty < \xi < +\infty \ (i = 1, 2), \tag{4}$$

$$\theta_1 = 1 \quad \text{if } \eta = 1 \ \forall\xi \leqslant 0, \tag{5}$$

$$\theta_2 = 0 \quad \text{if } \eta = 1 \ \forall\xi > 0, \tag{6}$$

$$\theta_1 = \theta_2 \quad \text{if } \xi = 0 \ \forall 0 \leqslant \eta < 1, \tag{7}$$

$$\frac{\partial\theta_1}{\partial\xi} = \frac{\partial\theta_2}{\partial\xi} \quad \text{if } \xi = 0 \ \forall 0 \leqslant \eta < 1. \tag{8}$$

Conditions (7) and (8) express the continuities of the temperature and the heat flux at the entrance section $\xi = 0$. For infinitely large values of $|\xi|(\xi \to \pm\infty)$, the dimensionless temperature is the particular solution of the following equation:

$$\frac{\partial^2\theta_i}{\partial\eta^2} = -BrD(M, \eta). \tag{9}$$

It is interesting to note that the dimensionless velocity profile

$$u(\eta) = \frac{2}{3}\frac{u_x(\eta)}{U_m}$$

is independent of the electric conductivity of the walls.

2.2. General form of the solution

For a given fully developed velocity profile $u(\eta)$, we propose a separation of variables method to generate the general solution of elliptic Eq. (3) in the upstream and downstream regions verifying the conditions (4)–(6) and (9). This solution can be represented by infinite series of eigenfunctions given by:

$$\theta_1(\xi, \eta) = 1 + \sum_{n=1}^{\infty} A_n f_n(\eta)\exp(\lambda_n^2\xi) + BrF(M, \eta) \quad \text{for } \xi \leqslant 0, \tag{10a}$$

$$\theta_2(\xi, \eta) = \sum_{n=1}^{\infty} B_n g_n(\eta)\exp(-\beta_n^2\xi) + BrF(M, \eta) \quad \text{for } \xi > 0 \tag{10b}$$

with

$$F(M, \eta) = d_0 + d_1\eta^2 + d_2\mathrm{ch}M\eta + d_3\mathrm{ch}2M\eta, \tag{11}$$

where the constants d_0, d_1, d_2 and d_3 are defined in terms of Hartmann number, M, and the parameter, χ, as (see [22])

$$\begin{aligned}
d_0 &= \chi^2\frac{M^2}{2} + \chi\frac{M(M^2-2)\mathrm{ch}M}{(M\mathrm{ch}M - \mathrm{sh}M)} + \frac{M^2(\mathrm{ch}^2M + (2M^2-8)\mathrm{ch}^2M)}{4(M\mathrm{ch}M - \mathrm{sh}M)^2},\\
d_1 &= -\chi^2\frac{M^2}{2} - \chi\frac{M^3\mathrm{ch}M}{(M\mathrm{ch}M - \mathrm{sh}M)}, -\frac{M^4\mathrm{ch}^2M}{2(M\mathrm{ch}M - \mathrm{sh}M)^2},\\
d_2 &= 2\chi\frac{M}{(M\mathrm{ch}M - \mathrm{sh}M)} + \frac{2M^2\mathrm{ch}M}{(M\mathrm{ch}M - \mathrm{sh}M)^2},\\
d_3 &= -\frac{M^2}{4(M\mathrm{ch}M - \mathrm{sh}M)^2}.
\end{aligned} \tag{12}$$

The λ_n and β_n designate the real eigenvalues associated with, respectively, the eigenfunctions f_n and g_n. A_n and B_n are the constants of integration. The eigenfunctions f_n and g_n are then the solutions of the following differential equations:

$$\frac{d^2 f_n}{d\eta^2} + \lambda_n^2 \left[\frac{\lambda_n^2}{Pe^2} - u(\eta) \right] f_n = 0, \tag{13a}$$

$$\frac{d^2 g_n}{d\eta^2} + \beta_n^2 \left[\frac{\beta_n^2}{Pe^2} + u(\eta) \right] g_n = 0 \tag{13b}$$

satisfying the boundary conditions:

$$f_n'(0) = 0 \quad \text{and} \quad f_n(1) = 0, \tag{14a}$$

$$g_n'(0) = 0 \quad \text{and} \quad g_n(1) = 0. \tag{14b}$$

The fundamental problem is then to determine the eigenvalues λ_n, β_n and the expansion coefficients A_n and B_n. From the boundary conditions (14a) and (14b) the eigenvalues must be roots of characteristic equations $f_n(1) = 0$ and $g_n(1) = 0$ from the boundary conditions (7), (8) we obtain the following equations with unknown expansion coefficients A_n and B_n:

$$1 + \sum_{n=1}^{\infty} A_n f_n(\eta) = \sum_{n=1}^{\infty} B_n g_n(\eta), \tag{15a}$$

$$\sum_{n=1}^{\infty} \lambda_n^2 A_n f_n(\eta) = -\sum_{n=1}^{\infty} \beta_n^2 B_n g_n(\eta). \tag{15b}$$

The eigenproblem (13a), (13b) and (14a), (14b) is different from the classical Sturm–Liouville problem, because the eigenvalues occur nonlinearly in (13a) and (13b). Consequently, the eigenfunctions are not orthogonal. Recently in [10], we have studied the extended Graetz problem with Poiseuille flow and we have presented a new procedure for the determination of the expansion coefficients A_n and B_n. This procedure has the advantage of giving the explicit forms of these coefficients for any arbitrary given developed flow in comparison with the other methods used earlier (variational method, Gramm–Schmidt procedure) and can be applied to other boundary conditions such as the Neumann or Robin boundary conditions. These coefficients can be written, by using (15a) and (15b), as (see [10]):

$$A_n = -\int_0^1 \left[\frac{\lambda_n^2}{Pe^2} - u(\eta) \right] f_n \, d\eta \Big/ \int_0^1 \left[\frac{2\lambda_n^2}{Pe^2} - u(\eta) \right] f_n^2 \, d\eta = 2 \Big/ \lambda_n \frac{\partial f_n(1)}{\partial \lambda} \Big|_{\lambda=\lambda_n}, \tag{16a}$$

$$B_n = \int_0^1 \left[\frac{\beta_n^2}{Pe^2} + u(\eta) \right] g_n \, d\eta \Big/ \int_0^1 \left[\frac{2\beta_n^2}{Pe^2} + u(\eta) \right] g_n^2 \, d\eta = -2 \Big/ \beta_n \frac{\partial g_n(1)}{\partial \beta} \Big|_{\beta=\beta_n}. \tag{16b}$$

It is interesting to note that the solution of the problem with Dirichlet wall boundary conditions in the absence of heat generation ($Br = 0$) will always be expressed in the forms given by the first terms of (10a), (10b) and Eqs. (16a) and (16b) for any given fully developed flow, and can be applied to non-Newtonian fluids for example.

For large values of Peclet number ($Pe \to \infty$) and when $M = 0$ and $Br = 0$ the solution (10a) and (10b) tends to the classical Graetz problem without axial conduction, since the eigenvalues β_n tend to those of the ordinary Graetz problem, given by Eq. (13b), where $Pe \to \infty$; the eigenvalues λ_n go to infinity, and from Eqs. (16a) and (10a) $\theta_1(\xi, \eta)$ tends to 1 (a flat temperature profile) in the upstream region.

The dimensionless bulk temperature $\theta_{b,i}(\xi)$ and the local Nusselt number $Nu_i(\xi)$ (constructed by hydraulic diameter) can now be defined and obtained in the upstream and downstream regions, by:

$$\theta_{b,i}(\xi) = \frac{\int_0^1 u(\eta)\theta_i \, d\eta}{\int_0^1 u(\eta) \, d\eta}, \tag{17}$$

$$Nu_i = -\frac{4 \frac{\partial \theta_i}{\partial \eta}\Big|_{\eta=1}}{\theta_{b,i} - \theta_i(\eta = 1)} \quad (i = 1, 2). \tag{18}$$

Substituting Eq. (17) into Eq. (18) by using Eqs. (10b) and (13b), we can deduct the expression of local Nusselt number in the downstream region:

$$Nu(\xi) = Nu_2 = \frac{8}{3}\frac{\sum_{n=1}^{\infty} B_n g_n'(1)\exp(-\beta_n^2\xi) + BrF'(M,1)}{\sum_{n=1}^{\infty} B_n \exp(-\beta_n^2\xi)\left[(g_n'(1)/\beta_n^2) + (\beta_n^2/Pe^2)\int_0^1 g_n(\eta)\,\mathrm{d}\eta\right] - Br\int_0^1 u(\eta)F(M,\eta)\,\mathrm{d}\eta} \quad \text{if } \xi > 0. \tag{19}$$

The terms multiplied by Br in (19) can be evaluated as

$$F'(M,1) = -\chi^2 M^2 - 2\chi M^2 - \frac{M^3 \mathrm{ch}M}{(M\mathrm{ch}M - \mathrm{sh}M)}, \tag{20}$$

$$\int_0^1 u(\eta)F(M,\eta)\,\mathrm{d}\eta = \frac{2M}{3(M\mathrm{ch}M - \mathrm{sh}M)}\left\{d_0\left(\mathrm{ch}M - \frac{\mathrm{sh}M}{M}\right) + d_1\left[\frac{chM}{3} - \frac{(M^2+2)\mathrm{sh}M}{M^3} + \frac{2\mathrm{ch}M}{M^2}\right] + d_2\left(\frac{\mathrm{sh}2M}{4M} - \frac{1}{2}\right) + d_3\left[\frac{\mathrm{sh}2M\mathrm{ch}M}{2M} - \frac{\mathrm{sh}M}{2M} - \frac{\mathrm{sh}3M}{6M}\right]\right\}. \tag{21}$$

Notice that for $Br = 0$ the asymptotic value of the local Nusselt number $Nu_{\mathrm{as.}}$, corresponding to the thermally developed flow $\xi \to \infty$ without heat generation, can be obtained by keeping only the first term of the series of equation (19)

$$Nu_{\mathrm{as.}} = \frac{8}{3}\beta_1^2 \Bigg/ \left[1 + \frac{\beta_1^4\int_0^1 g_1(\eta)\,\mathrm{d}\eta}{Pe^2 g_1'(1)}\right]. \tag{22}$$

and for $Br \neq 0$ the asymptotic value of the Nusselt number becomes independent of both Brinkman number and Peclet number when viscous and Joule dissipation are included in the analysis and can be written as

$$Nu_{\mathrm{as.}} = -\frac{8}{3}\frac{F'(M,1)}{\int_0^1 u(\eta)F(M,\eta)\,\mathrm{d}\eta}. \tag{23}$$

2.3. Eigenfunctions for Hartmann flow

It is noted that when $M = 0$, one obtains $u(\eta) = 1 - \eta^2$ (Hagen–Poiseuille flow) and the eigenfunctions correspond to confluent hypergeometric functions which are given explicitly in [10].

For $M \neq 0$, let us examine the solution of the differential equations (13a) and (13b) for the boundary conditions (14a) and (14b) in the case of Hartmann flow. We introduce new variables and parameters:

$$z = \frac{M\eta}{2}, \quad q_0 = \frac{4Pe^2}{9M^2\mathrm{ch}M[1 - (\mathrm{th}M/M)]^2}, \quad a = q\mathrm{ch}M\left(2 - \frac{q}{q_0}\right), \tag{24}$$

and a new function:

$$h_n(z) = \begin{cases} g_n(z) & \text{if } q = -4\beta_n^2/3M^2\mathrm{ch}M(1 - (\mathrm{th}M/M)), \\ f_n(z) & \text{if } q = 4\lambda_n^2/3M^2\mathrm{ch}M(1 - (\mathrm{th}M/M)). \end{cases} \tag{25}$$

Eqs. (13a) and (13b) are then grouped and transformed to a new differential equation verified by $h_n(z)$

$$\frac{\mathrm{d}^2 h_n}{\mathrm{d}z^2} - (a - 2q\mathrm{ch}2z)h_n = 0 \tag{26}$$

with the boundary conditions

$$\frac{\mathrm{d}h_n}{\mathrm{d}z}(0) = 0 \quad \text{and} \quad h_n\left(\frac{M}{2}\right) = 0. \tag{27}$$

Eq. (26) corresponds to a standard form of Mathieu's modified differential equation with real parameters a and q [24]. An algorithm for the computation of Eq. (26) over a wide range of parameters a, q and z does not seem to exist. Computational difficulties arise as q and a become large precisely for large order n of eigenvalues. Therefore in the next two sections we obtain the appropriate analytical solutions for small and large values of parameter q.

3. Analytical solution

3.1. Solution for small value of q

Let us formally assume the possibility to express the solution by an expansion in terms of the parameter q as

$$h_n(z) = \sum_{m=0}^{\infty} q^m V_m(a,z), \tag{28}$$

then the functions V_m satisfy the following recurrence differential equations:

$$\begin{cases} V_0'' - aV_0 = 0, \\ V_m'' - aV_m = -2\mathrm{ch}2z\ V_{m-1}, \quad m = 1,2,3,\ldots \end{cases} \tag{29}$$

So, after several iterations and integration of Eq. (29), we can built a general form of the solution for $a \neq 0$ and $q \neq 0$ not integers as follows:

$$\begin{aligned} h_n(z) = {} & \sum_{p=0}^{\infty}\sum_{n=0}^{\infty} q^{4p+n} z^{2p} \left(A^n_{0,4p+n} \mathrm{ch} z\sqrt{a} + q^2 C^n_{0,4p+n} z \mathrm{sh} z\sqrt{a} \right) \\ & + \sum_{p=0}^{\infty}\sum_{n=1}^{\infty}\sum_{k=0}^{n-1} q^{4p+n} z^{2p} \Big\{ A^n_{-(n-k),4p+n} \mathrm{ch}(\sqrt{a} - 2(n-k))z + A^n_{n-k,4p+n} \mathrm{ch}(\sqrt{a} + 2(n-k))z \\ & + q^2 z \Big[C^n_{-(n-k),4p+n} \mathrm{sh}(\sqrt{a} - 2(n-k))z + C^n_{n-k,4p+n} \mathrm{sh}(\sqrt{a} + 2(n-k))z \Big] \Big\}. \end{aligned} \tag{30}$$

The hyperbolic functions ch, sh and the coefficients $A^n_{m,4p+n}$, $C^n_{m,4p+n}$ are complex numbers if $a < 0$ or reals if $a > 0$. If we report (30) in (26) we obtain some recurrence relation formulas which determine these coefficients. These recurrence relations are given in Appendix A. Since, the parameter q is small, the series (30) is rapidly convergent and can be truncated to order 6 as

$$h_n(z) = V_0 + qV_1 + q^2V_2 + q^3V_3 + q^4V_4 + q^5V_5 + q^6V_6 + \mathrm{O}(q^7) \tag{31}$$

with

$$\begin{aligned} V_0 &= A^0_{0,0} \mathrm{ch} z\sqrt{a}, \\ V_1 &= \sum_{k=-1}^{1} A^1_{k,1} \mathrm{ch}(\sqrt{a} + 2k)z, \\ V_2 &= \sum_{k=-2}^{2} A^2_{k,2} \mathrm{ch}(\sqrt{a} + 2k)z + C^0_{0,0} z \mathrm{sh}(\sqrt{a}z), \\ V_3 &= \sum_{k=-3}^{3} A^3_{k,3} \mathrm{ch}(\sqrt{a} + 2k)z + \sum_{k=-1}^{1} C^1_{k,1} z \mathrm{sh}(\sqrt{a} + 2k)z, \\ V_4 &= \sum_{k=-4}^{4} A^4_{k,4} \mathrm{ch}(\sqrt{a} + 2k)z + \sum_{k=-2}^{2} C^2_{k,2} z \mathrm{sh}(\sqrt{a} + 2k)z + A^0_{0,4} z^2 \mathrm{ch}(\sqrt{a}z), \\ V_5 &= \sum_{k=-5}^{5} A^5_{k,5} \mathrm{ch}(\sqrt{a} + 2k)z + \sum_{k=-1}^{1} A^1_{k,5} z^2 \mathrm{ch}(\sqrt{a} + 2k)z + \sum_{k=-3}^{3} C^3_{k,3} z \mathrm{sh}(\sqrt{a} + 2k)z, \\ V_6 &= \sum_{k=-6}^{6} A^6_{k,6} \mathrm{ch}(\sqrt{a} + 2k)z + \sum_{k=-2}^{2} A^2_{k,6} z^2 \mathrm{ch}(\sqrt{a} + 2k)z + \sum_{k=-4}^{4} C^4_{k,4} z \mathrm{sh}(\sqrt{a} + 2k)z + C^0_{0,4} z^3 \mathrm{sh}(\sqrt{a}z) \end{aligned} \tag{32}$$

and the coefficients appearing in (32) should be determinate and are given explicitly in Appendix B.

3.2. Solution for large value of q

For very large values of parameter q which correspond to the case of very large eigenvalues, the asymptotic solution of Eq. (26) in this case can be obtained by invoking the Wentzel–Kramers–Brillouin (WKB) approximation. By replacing z by η we have

$$h_n(\eta) = \left[\frac{a-2q}{a-2q\mathrm{ch}M\eta}\right]^{1/4} \cos\Omega_n(\eta) \quad \text{for } 0 \leqslant \eta \leqslant 1, \tag{33}$$

where

$$\begin{aligned}\Omega_n(\eta) &= \frac{1}{2}\int_0^{M\eta} [2q\mathrm{ch}t - a]^{1/2}\,\mathrm{d}t \\ &= \begin{cases} [-(a+2q)]^{1/2}\left[F\left(\frac{\pi}{2},k\right) - F(\varphi,k) + E(\varphi,k) - E\left(\frac{\pi}{2},k\right)\right] & \text{if } h_n(\eta) = g_n(\eta), \\ [2q-a]^{1/2}\left[F\left(\phi,\frac{1}{k}\right) - E\left(\phi,\frac{1}{k}\right)\right] + \mathrm{th}\left(\frac{M\eta}{2}\right)[2q\mathrm{ch}M\eta - a]^{1/2} & \text{if } h_n(\eta) = f_n(\eta) \end{cases}\end{aligned} \tag{34}$$

with

$$k = \left[\frac{a-2q}{a+2q}\right]^{1/2}, \quad \varphi = \arcsin\left[\frac{a-2q\mathrm{ch}M\eta}{a-2q}\right]^{1/2} \quad \text{and} \quad \phi = \arcsin\left[\mathrm{th}\left(\frac{M\eta}{2}\right)\right]. \tag{35}$$

Eq. (33) is not a good approximation to the solution near the wall for $Pe \to \infty$, ($q_0 \to \infty$) and $\eta \to 1$, since it has a singularity there because $a \to 2q\mathrm{ch}M$, but it is clear that for finite value of Peclet number Eq. (33) is valid near the wall ($\eta \to 1$).

To satisfy the boundary condition $h_n(1) = 0$, thus, we derive the asymptotic transcendental formula for the large eigenvalues

$$\Omega_n(1) = \pi\left(n - \frac{1}{2}\right), \quad n = 1, 2, 3\ldots \tag{36}$$

The roots of Eq. (36) represent, therefore, the desired asymptotic eigenvalues for finite Peclet number. From Eq. (33), the asymptotic expression for the derivative of the eigenfunctions in the downstream region at the wall can be found to be

$$g_n'(1) = (-1)^n \frac{\beta_n^{3/2}}{Pe^{1/2}}\left[\frac{2(\mathrm{ch}M - 1)}{3(\mathrm{ch}M - (\mathrm{sh}M/M))} + \frac{\beta_n^2}{Pe^2}\right]^{1/4}. \tag{37}$$

For large Peclet number $Pe \to \infty$, the effect of axial heat conduction can be neglected and the uniform asymptotic expression for $g_n(\eta)$ can be established by using similar analysis used by Sellars et al. [25] and Housiadas et al. [26] for electrically nonconducting fluids ($M = 0$). We provide a WKB asymptotic expansion valid for $0 \leqslant \eta < 1$ ($g_n^0(\eta)$) and an approximation to the exact solution valid for η near the wall ($g_n^1(\eta)$), as follows:

$$g_n^0(\eta) = \left[\frac{\mathrm{ch}M - 1}{\mathrm{ch}M - \mathrm{ch}M\eta}\right]^{1/4} \cos\Omega_n(\eta) \quad \text{for } 0 \leqslant \eta < 1, \tag{38}$$

$$g_n^1(\eta) = (-1)^{n-1}\frac{2^{1/4}}{3^{3/4}}(\pi\beta_n)^{1/2}\left[\frac{\mathrm{ch}M - 1}{\mathrm{ch}M - (\mathrm{sh}M/M)}\right]^{1/4}(1-\eta)^{1/2}J_{1/3}\left[\left(\frac{2}{3}\right)^{3/2}\beta_n\left[\frac{M\mathrm{th}M}{1-(\mathrm{th}M/M)}\right]^{1/2}(1-\eta)^{3/2}\right], \tag{39}$$

where $J_{1/3}$ is the Bessel function of the first kind. The characteristic equation for the eigenvalues in the case of $Pe \to \infty$, becomes

$$\Omega_n(1) = \pi\left(n - \frac{7}{12}\right), \quad n = 1, 2, 3\ldots \tag{40}$$

By using the method of asymptotic matching of the piecewise WKB approximation and some intermediate results, we established the following matching function that connect (38) and (39)

$$g_n^{0,1}(\eta) = \left[\frac{\mathrm{ch}M - 1}{M\mathrm{sh}M}\right]^{1/4}\frac{1}{(1-\eta)^{1/4}}\cos\left[\Omega_n(1) - \left(\frac{2}{3}\right)^{3/2}\beta_n\left[\frac{M\mathrm{th}M}{1-(\mathrm{th}M/M)}\right]^{1/2}(1-\eta)^{3/2}\right]. \tag{41}$$

The asymptotic formula for the eigenfunctions uniform throughout the whole interval $0 \leqslant \eta \leqslant 1$ can be written as

$$g_n(\eta) = g_n^0(\eta) + g_n^1(\eta) - g_n^{0,1}(\eta). \tag{42}$$

The expressions of the large eigenvalues, the derivative of the eigenfunctions at the wall and the expansion coefficients B_n in Eq. (16b), for $Pe \to \infty$, can be written as

$$\beta_n = 3^{1/2}M\left(\mathrm{ch}M - \frac{\mathrm{sh}M}{M}\right)^{1/2}\left(n\pi - \frac{7\pi}{12}\right)\Big/ 2^{3/2}(\mathrm{ch}M+1)^{1/2}\left[F\left(\frac{\pi}{2},k\right) - E\left(\frac{\pi}{2},k\right)\right], \quad n = 1,2,3\ldots, \tag{43}$$

$$g_n'(1) = (-1)^n \frac{2^{5/12}}{3^{5/4}\Gamma(4/3)}(\pi)^{1/2}\left[\frac{\mathrm{ch}M-1}{\mathrm{ch}M-(\mathrm{sh}M/M)}\right]^{1/4}\left[\frac{M\mathrm{th}M}{1-(\mathrm{th}M/M)}\right]^{1/6}\beta_n^{5/6}, \quad n = 1,2,3\ldots, \tag{44}$$

$$B_n = \frac{(-1)^{n+1}2^{-19/12}3^{5/4}\Gamma(2/3)M}{(\pi)^{1/2}\left[F\left(\frac{1}{2}\pi,k\right) - E\left(\frac{1}{2}\pi,k\right)\right]}\left[\frac{\mathrm{ch}M-(\mathrm{sh}M/M)}{\mathrm{ch}M-1}\right]^{1/4}\left[\frac{\mathrm{ch}M-(\mathrm{sh}M/M)}{\mathrm{ch}M+1}\right]^{1/2}\left[\frac{M\mathrm{th}M}{1-(\mathrm{th}M/M)}\right]^{1/6}\beta_n^{-7/6}. \tag{45}$$

When $M \to 0$ one can easily verify that Eqs. (43)–(45) tend to the solution of original analysis of Sellars et al. [25] for nonconducting fluid and when axial conduction is negligible ($Pe \to \infty$). Indeed when $M \to 0$,

$$k = \left[\frac{\mathrm{ch}M-1}{\mathrm{ch}M+1}\right]^{1/2} \to 0,$$

the elliptic integrals for small k can be written as

$$E\left(\frac{\pi}{2},k\right) \approx \frac{\pi}{2} - k^2\frac{\pi}{8}$$

and

$$F\left(\frac{\pi}{2},k\right) \approx \frac{\pi}{2} + k^2\frac{\pi}{8}.$$

Thus the constants β_n, $g_n'(1)$ and B_n for $M = 0$ can be simplified as follows:

$$\beta_n = 4n - (7/3), \quad n = 1,2,3\ldots, \tag{46}$$

$$g_n'(1) = \frac{(-1)^n 2^{1/6}(\pi)^{1/2}}{3^{5/6}\Gamma(4/3)}\beta_n^{5/6}, \tag{47}$$

$$B_n = \frac{(-1)^{n+1}}{\pi^{3/2}}\Gamma(2/3)3^{2/3}2^{13/6}\beta_n^{-7/6}. \tag{48}$$

hese results are in agreement with the analytical results of Sellars et al.

4. Results and discussions

We performed our analysis for $Pe = 1.5$, 5, 15, ∞ with various values of Hartmann number $M = 0$, 5, 10, 50, Brinkman number $Br = 0$, 0.1, 1, over the range of axial distances $10^{-4} \leqslant \xi \leqslant 10$ under electrically insulating wall conditions, $\chi = -1$ and perfectly conducting wall condition, $\chi = 0$. It is emphasized that these are the first results in the literature obtained for axial distance $\xi \geqslant 10^{-4}$ not only for thermal entrance region of MHD channel but also for entrance region without applied magnetic field.

The eigenvalues λ_n and β_n zeros of Mathieu's functions have been numerically computed using a Newton–Raphson algorithm. The derivatives and the integrals appearing in expressions (16a), (16b), (19), (22) and (23) giving the important constants, the local and asymptotic Nusselt numbers have been calculated analytically by derivation and integration of Mathieu's functions.

The validity of our analytical solution is verified by the comparison presented in Table 1, between the eigenvalues β_n in the downstream region obtained from the present analysis and those calculated by LeCroy and Eraslan [22] using the Galerkin method (β_n and Pe in the present definition are equivalent to $\sqrt{(3/2)\beta_n^*}$ and $(3/2)Pe^*$, respectively, in LeCroy's definition). It is clear from this table that the eigenvalues agree very well with the previous investigation. The results are identical to five decimal places. Table 1 also presents the results obtained from the WKB approximation of the present analysis given by Eqs. (36) and (40). It is also clear from this table that for small and moderate Peclet numbers the absolute errors $|\beta_n - [\beta_n]_{\mathrm{asymp.}}|$ between results obtained from solution (31) and asymptotic WKB approximation given by Eq. (36) decrease as n increases and the asymptotic evaluation by WKB of the eigenfunctions is successful for large n. The two results agree very well with eight decimal places for $n \geqslant 500$ for $Pe = 1.5$ and 5. However, for very large Peclet number ($Pe \to \infty$), with increasing n, the absolute errors increase and ultimately become unacceptable, so solution (31) becomes inaccurate for very large order n. In conclusion, for small Peclet number solution (31) can be used without

Table 1
Eigenvalues in the downstream region for $M = 10$ with various values of Peclet number and comparison with the results of LeCroy and Eraslan [22]

Pe	n	β_n (present work)	β_n [22]	$[\beta_n]_{\text{asymp.}}$ (present work)	$\lvert\beta_n - [\beta_n]_{\text{asymp.}}\rvert$
1.5	1	1.2926202	1.2926194	1.3138492	0.021
	2	2.5136936	2.5136915	2.5218913	0.0082
	3	3.3214605	3.3214598	3.3250405	0.0036
	4	3.9682137	3.9682112	3.9700369	0.0018
	15	8.2208848	8.2209124	8.2209462	0.00006
	16	8.5026574	8.5027378	8.5027094	0.00005
	500	48.50864274		48.50864275	10^{-8}
	1000	68.6242147375		68.624214736	10^{-9}
5	1	1.7035538		1.7754100	0.072
	2	4.0411310		4.0865206	0.045
	3	5.6208263		5.6429016	0.022
	4	6.8655426		6.8772988	0.012
	500	88.53134447		88.53134452	5×10^{-8}
	1000	125.26682830		125.26682832	2×10^{-8}
15	1	1.8152752	1.8152727	1.9192628	0.10
	2	5.1836868	5.1836811	5.3262302	0.14
	3	7.9679554	7.9679514	8.0654224	0.097
	4	10.2622276	10.262222	10.3236818	0.061
	15	24.7478461	24.754999	24.7502003	0.023
∞	1	1.8332912	1.8332880	1.6203594	0.21
	2	5.6037011	5.6036863	5.5092219	0.094
	3	9.4547859	9.4547845	9.3980844	0.057
	4	13.3275014	13.3274530	13.2869469	0.040
	5	17.2074411	17.207426	17.1758093	0.032
	6	21.0906320	21.0906260	21.0646718	0.026
	11	40.5242094		40.5089843	0.015
	20	75.92592003		75.5087468	0.417
	50	193.6858525		192.1746216	1.51

resorting to the WKB approximation, while for very large Peclet number the WKB approximation becomes unavoidable beyond some order n and the calculation in this case can be optimized by suitably combining the two solutions.

Notice that although the eigenvalues in the downstream region of the problem of an infinite axial region studied here are the same as the eigenvalues of the problem of semi-infinite region [22], the solution for the two problems is different for small Peclet number, because the expansion coefficients B_n in Eq. (16b) are different for the two problems and depend on the entrance boundary conditions at $\xi = 0$. This difference also exists for nonconducting fluid ($M = 0$). However, when $Pe \to \infty$ the two solutions are identical.

Note that the infinite series in Eqs. (10a) and (10b), representing the temperature field in the upstream and downstream regions of the entrance section of heat transfer $\xi = 0$, converge very slowly and require a high number of terms, especially for low values of Peclet number. This difficulty is due to a slow decrease of the expansion coefficients A_n and B_n of the series. In this study, we have calculated the temperature profiles and the local Nusselt numbers using 1000 terms in the series (10a), (10b) and (19) which allows a satisfactory convergence and a good matching at $\xi = 0$ for the temperature between upstream and downstream region where their comparison is used as the criterion of convergence [10]. Indeed, if only a few terms have been used for evaluating the series for example of 20 terms, it causes considerable errors and shows poor matching of the temperature and gives erroneous results in the prediction of local Nusselt number near $\xi = 0$. Similar results have been reported by the authors in [10]. The interest in the use of 1000 terms for small Peclet numbers is shown and demonstrated in Fig. 2. This figure illustrates the effect of different truncation orders N of the series in Eq. (19) on the accuracy of a local Nusselt number for $Br = 0$, $M = 10$, $Pe = 5$ and $Pe = \infty$. The curves of different values of N, indicate the improved convergence level of local Nusselt number. Clearly, the accuracy or relative errors of Nusselt number is improved and convergence is achieved with a very high number of terms and requiring an increase in N as ξ is decreased. Relative error between curve of $N = 1000$ for $Pe = 5$ and curves of $N = 900$,

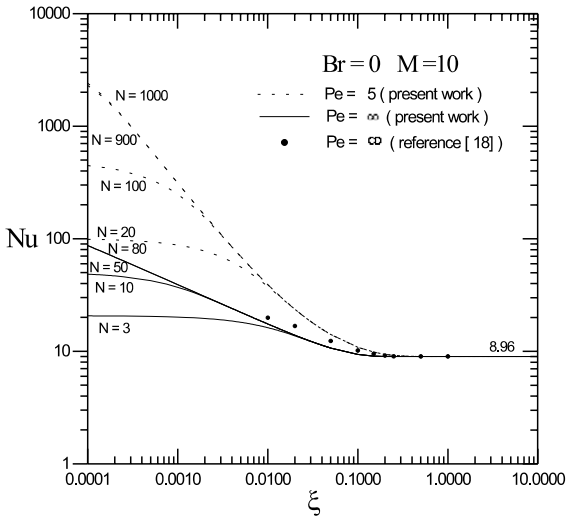

Fig. 2. Effect of different truncation orders N on the accuracy of a local Nusselt number for $Br = 0$, $M = 10$, $Pe = 5$ and $Pe = \infty$ and comparison with the results of Nigam and Singh [18].

100 and 20 are, around $\xi = 10^{-4}$, of the order of 4% for $N = 900$, 81% for $N = 100$ and 96% for $N = 20$. The choice of 20 terms, for example, in evaluating Nusselt number is therefore recommended only for axial distances $\xi \geqslant 10^{-2}$ for $Pe = 5$. Similar trends can be observed for $Pe = \infty$. The merging of the two curves for $N = 50$ and 80 indicates that the convergence of Nusselt number is achieved with $N = 50$ around $\xi = 10^{-4}$. The comparison between the two curves for $Pe = 5$ and ∞ with the same value of M indicates that the axial conduction effect disappears completely at $\xi = 0.3$. Fig. 2 also shows a comparison of the local Nusselt number, obtained in this work with results of Nigam and Singh [18] in the case of negligible axial heat conduction ($Pe = \infty$) which used $N = 3$ terms in evaluating Nusselt number where the expansion coefficients were calculated approximately by variational method (Nu in the present definition is equivalent to $4Nu^*$ in Nigam's definition). The results are in agreement with data of these authors for axial distance $\xi \geqslant 0.2$, but for $\xi < 0.2$ there exists a substantial difference between the two results due to inaccuracies in Nigam's numerical values of expansion coefficients B_n.

4.1. Main results for $Br = 0$

The typical radial dimensionless temperature profiles

$$\theta_i = \frac{T_i - T_f}{T_0 - T_f}, \quad i = 1, 2$$

with the dimensionless axial coordinate, $\xi = x/bPe$ for strong axial heat conduction $Pe = 5$, by neglecting viscous and Joule dissipation, $Br = 0$ and various values of Hartmann number $M = 0$, 5, 10, 50 are presented in Fig. 3. The figure also presents the results of the case of no applied magnetic field $M = 0$ given from the analytical solution of reference [10]. It can be seen that the temperature profiles retain globally the same shape as in the absence of magnetic field. It is also shown that when M increases, the dimensionless temperature θ is reduced in the central core of the channel for the whole range of ξ. On the contrary, outside the core, at the external part of the flow the temperature distribution tends to be higher when M increases. This is particularly sensitive in the section corresponding to high temperature level (the entrance region $\xi \leqslant 0.05$). The decay of θ in the central core could be attributed to decay of the velocity field in this region due to Hartmann effect. Outside the core the velocity is increased by the magnetic field, due to the global conservation of the flow rate. In these regions then, the level of temperature tends to decrease when the Hartmann number increases. Indeed, when M increases and reaches the value 50, the velocity profile becomes almost uniform and tends to a slug flow (see Fig. 4) in the whole diameter of the channel except near the wall characterized by the well known Hartmann layer and a strong velocity gradient. Besides one can notice from Fig. 3 that the temperature gradient does not appear to be affected by the magnetic field. This could be explained by the fixed value of the mean velocity U_m, identical for all the presented results, corresponding to identical values of the flow rate which controls for the essential heat exchange in the absence of internal source.

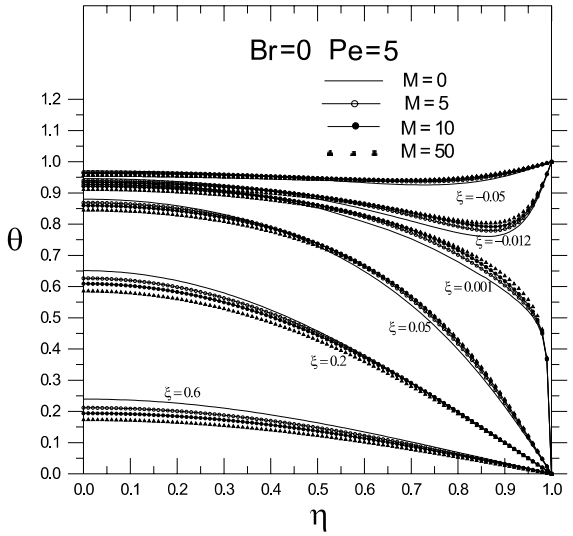

Fig. 3. Radial dimensionless temperature profiles for $Br = 0$, $Pe = 5$, for various values of axial distance ξ and Hartmann number M.

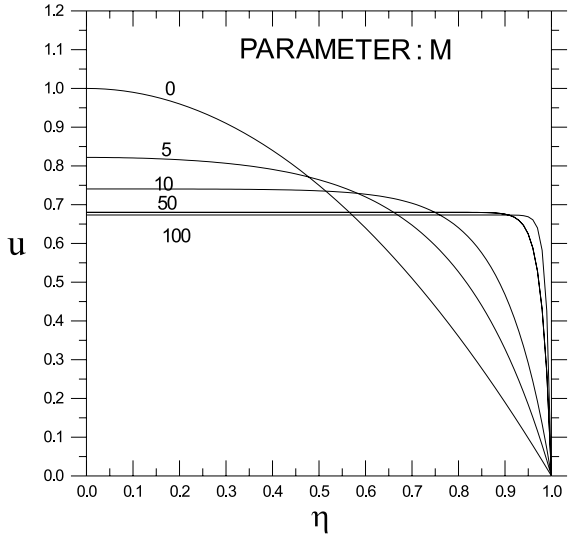

Fig. 4. Dimensionless velocity profiles of Hartmann flow for various values of Hartmann number M.

The effect of magnetic field on local Nusselt number, corresponding to $Br = 0$, is shown in Fig. 5. It is noted that Nu decreases monotonically along the axial coordinates ξ and increases as M increases. This can be explained by the decay of bulk temperature θ_b at any point ξ due to Hartmann effect. The heat flux transmitted to the wall being almost unchanged when the Hartmann number increases, and the decay of the bulk temperature used as reference level for the definition of the Nusselt number (see Eq. (18)) correspond to an improvement of the Nusselt number. This is in line with the result of laminar hydrodynamic heat transfer, without magnetic field, in which the asymptotic Nusselt number is considerably smaller in Poiseuille flow than in slug flow, Bejan [27]. Similar tendencies have already been pointed out by several authors [18–23].

4.2. Main results for $Br \neq 0$

The developing radial temperature profiles at various axial positions in the thermal entrance region for positive value of Brinkman number $Br = 0.1$ (under cooling condition) in the case of $\chi = -1$ (insulating walls) and the case of $\chi = 0$

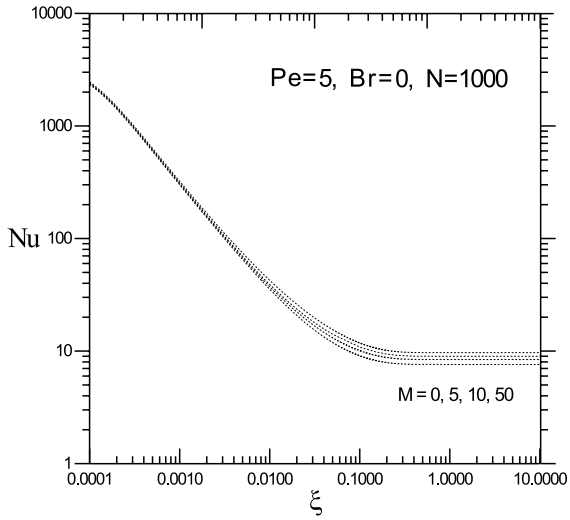

Fig. 5. Influence of magnetic field on the local Nusselt number for $Pe = 5$ and $Br = 0$.

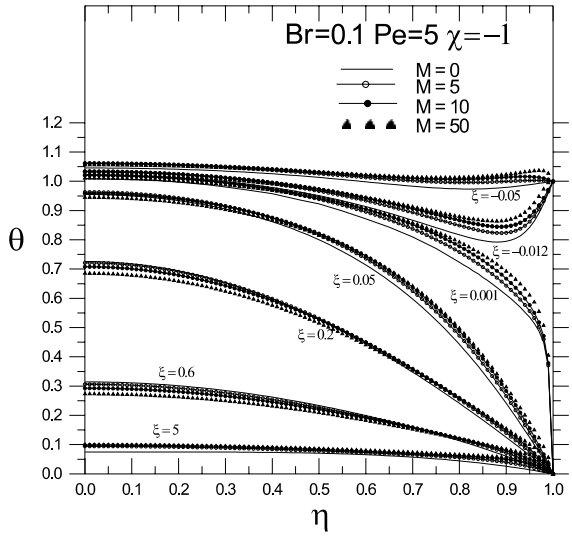

Fig. 6. Radial dimensionless temperature profiles for $Br = 0.1$, $Pe = 5$ under short circuit condition $\chi = -1$, for various values of axial distance ξ and Hartmann number M.

(perfectly conducting walls) are illustrated in Figs. 6 and 7, respectively. Fig. 8 also shows the influence of M on local Nusselt number variations in the two cases $\chi = -1$ and 0. It is seen that under insulating wall conditions and for $Br = 0.1$, the temperature profiles retain the same forms as in the case of $Br = 0$, while under perfectly conducting wall conditions the temperature profiles are completely different. The curves for $Br = 0.1$ and $M \neq 0$ represent the effect of heating by Joule and viscous dissipation while the curve for $Br = 0.1$ and $M = 0$ represents the effect of heating by viscous dissipation only.

For $Br = 0.1$ and $\chi = -1$ which represents the minimum of Joule heating condition in the central core of the channel, the influence of Hartmann number on the heat transfer is determined by the association of two different effects which act in the opposite sense: the Hartmann effect previously discussed and the effect of heating by Joule and viscous dissipation. The first effect acts to decrease the fluid temperature in the central core of the channel while the second acts to increase it. Then, globally, the temperature is improved compared with the case without magnetic field producing an increase of the temperature gradient at the walls and then an improvement of the heat transfer. This effect is particularly

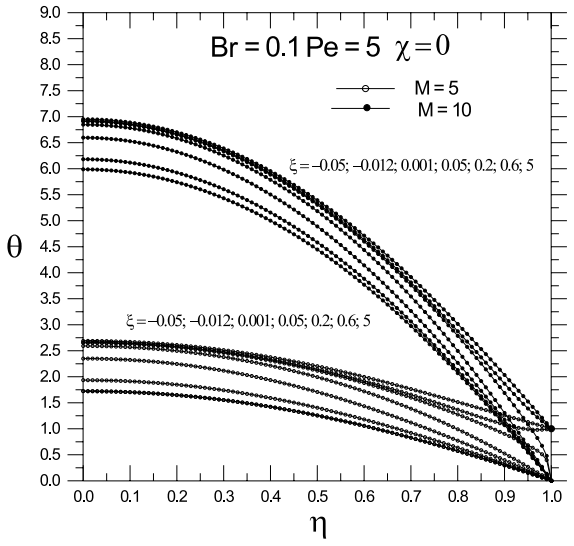

Fig. 7. Radial dimensionless temperature profiles for $Br = 0.1$, $Pe = 5$ under short circuit condition $\chi = 0$, for various values of axial distance ξ and Hartmann number M.

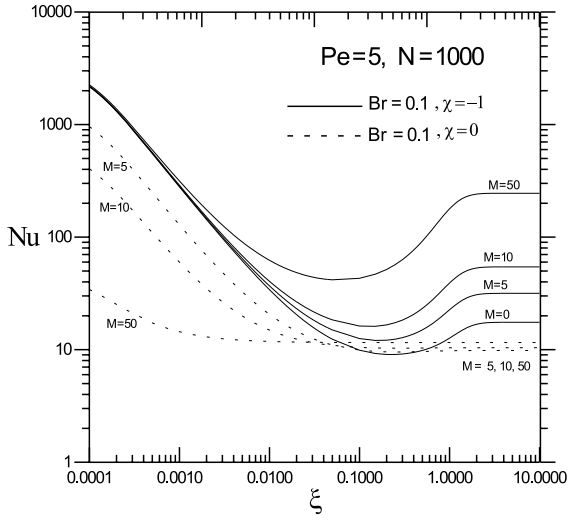

Fig. 8. Influence of magnetic field on the local Nusselt number for $Pe = 5$ and $Br = 0.1$ under open circuit $\chi = -1$ and short circuit, $\chi = 0$ conditions.

sensitive far from the entrance region where the level of temperature is low and consequently where the influence of the Joule and viscous source becomes important. It dominates the heat transfer in the thermally developed region for $\xi > 0.05$ (see Fig. 6).

For $Br = 0.1$ and $\chi = 0$ which represents strong Joule heating condition everywhere in the flow, the Hartmann effect (that means the influence of the velocity profile) becomes negligible and the heat transfer is dominated by Joule dissipation effect. Fig. 7 shows that the fluid temperature and the temperature gradient at the wall increase more and more when M is increasing. Fig. 8 also shows that for $\chi = 0$, the local Nusselt number decreases as M increases up to a certain axial distance $\xi \approx 0.03$ and the trend is opposite to that for $\xi > 0.03$. This can be explained from the variations of the wall gradient temperature and the bulk temperature in the axial direction. Indeed, from Fig. 7, it is noted that near the entrance section for $\xi \approx 0.001$ for example with an increase of M, the fluid temperature at the center of the channel for $M = 10$ is larger than for $M = 5$. This also means that the bulk temperature θ_b becomes larger for $M = 10$. While, the

temperature gradient in the two cases is of the same order for $\xi \approx 0.001$. Thus the bulk temperature increases and Nu decreases with an increase of M near the entrance section by considering the definition of

$$Nu = -\frac{4(\partial\theta/\partial\eta)|_{\eta=1}}{\theta_b}.$$

For increasing ξ, for example at $\xi \approx 0.6$ the temperature gradient and the bulk temperature are larger for $M = 10$ than for $M = 5$. However, the increase of $\partial\theta/\partial\eta|_{\eta=1}$ is larger than that of θ_b. Consequently, Nu increases slowly with an increase of M in the thermally fully developed region.

Fig. 8, for $Br = 0.1$ and $\chi = -1$ for minimum of Joule heating condition, shows that Nu does not decrease monotonically along the axial coordinate. The evolution of the Nusselt number along the flow presents a minimum value near the entrance region. This can be explained by the fact that, due to the Joule effect, the bulk temperature decrease more slowly than the heat exchange at the wall which decreases monotonically. After this first stage of evolution, the decreasing of the wall heat transfer along the flow becomes lower than the decreasing of the bulk temperature corresponding to an increasing of the Nusselt number which stabilizes at a fix value (which depends on the Hartmann number) when the equilibrium between the Joule heating and the heat transfer at the wall is reached. This asymptotic value of the Nusselt number increases when the Hartmann number increases. Fig. 9 compares the evolution of the Nusselt number along the flow direction for insulating wall ($\chi = -1$) and for two different values of the Brinkman number Br. It can be shown that the results are very similar and the presence of a minimum value for Nu can be well observed for $Br = 1$. But this effect is less important because in this situation the bulk temperature is more influenced by the Joule effect even at the vicinity of the entrance region. Then the equilibrium between Joule heating and heat transfer at the wall is obtained more rapidly and tends to vanish in the presence of the minimum value. The Nusselt number evolution becomes monotone for very large value of Br. It can be observed that the location of the minimum does not depend on the Brinkman number as well as the asymptotic value of the Nusselt number (according to the theoretical calculation expressed later). For strong Joule heating condition, $\chi = 0$, Nu exhibits a monotonically decreasing characteristic similar to the case of $Br = 0$. The results found for the asymptotic Nusselt number $Nu_{as.}$ contradict those obtained by LeCroy and Eraslan [22]. These authors have found that $Nu_{as.}$ for $\chi = 0$ is larger than $Nu_{as.}$ for $\chi = -1$ for fixed and large value of the Hartmann number. The characteristics of Nu in the cases of $\chi = -1$ and $\chi = 0$ (see Fig. 8) can be better understood by considering the definition of the asymptotic Nusselt number (i.e., thermally developed region) for $Br \neq 0$ and large values of the Hartmann number $M \gg 1$. Indeed, for the minimum Joule heating condition ($\chi = -1$), the fluid is little heated and we can show that for $M \gg 1$, the bulk temperature becomes of the order of

$$\theta_b \approx Br\left(\frac{\mathrm{th}^2 M}{3} + \frac{1}{2}\right) = \mathrm{O}(Br).$$

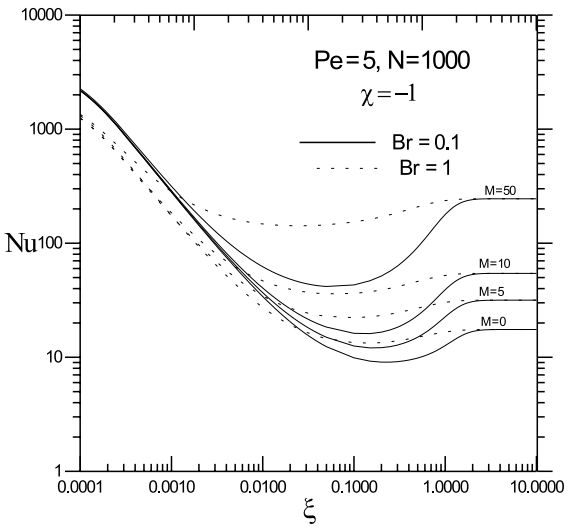

Fig. 9. Effect of Brinkman number Br and Hartmann number M on the local Nusselt number in the case of insulating walls for $Pe = 5$.

The temperature gradient at the wall increases proportionally to the Hartmann number for $M \gg 1$ as

$$\left.\frac{\partial\theta}{\partial\eta}\right|_{\eta=1} \approx -Br(M\mathrm{th}M + \mathrm{th}^2M) = \mathrm{O}(BrM).$$

Consequently the asymptotic Nusselt number increases proportionally to the Hartmann number as

$$Nu_{\mathrm{as.}} \approx \frac{4(M\mathrm{th}M + \mathrm{th}^2M)}{\frac{1}{3}\mathrm{th}^2M + \frac{1}{2}} = \mathrm{O}(M).$$

For the strong Joule heating condition ($\chi = 0$), the induced electrical current is considerable and the fluid is more heated by Joule effect, so the bulk temperature increases more than the previous case proportionally to M^2,

$$\theta_{\mathrm{b}} \approx Br\left(\frac{M^2}{3} + M\mathrm{th}M + 2\mathrm{th}^2M - \frac{5}{2}\right) = \mathrm{O}(BrM^2).$$

The temperature gradient also increases as M^2,

$$\left.\frac{\partial\theta}{\partial\eta}\right|_{\eta=1} \approx -Br(M^2 + M\mathrm{th}M + \mathrm{th}^2M) = \mathrm{O}(BrM^2).$$

Consequently $Nu_{\mathrm{as.}}$ varies poorly with respect to M and we have

$$Nu_{\mathrm{as.}} \approx \frac{4(M^2 + M\mathrm{th}M + \mathrm{th}^2M)}{\frac{1}{3}M^2 + M\mathrm{th}M + 2\mathrm{th}^2M - \frac{5}{2}} = \mathrm{O}(1).$$

Thus for large values of Hartmann number, $Nu_{\mathrm{as.}}$ for $\chi = -1$, is larger than $Nu_{\mathrm{as.}}$ for $\chi = 0$ and the results of Fig. 8 are justified and understood.

4.3. Application and examples

Two examples are illustrated in Figs. 10–12 to have some order of magnitude of the effect of magnetic field on the radial temperature profile in (°C) and on the local heat flux in ($\mathrm{MW/m^2}$) distribution with axial distance x in (m). This situation may be important for the study of the effect of low Peclet number of high temperature liquid metals with laminar regime in the presence of magnetic field and could occur in the nuclear reactors if the working fluid is slowed due to a pump malfunction. Sodium and lithium liquids with different characteristics of the flow are considered. In the case of sodium liquid (Figs. 10 and 12) at $T_0 = 538$ °C, and $T_{\mathrm{f}}) = 427$ °C with physical properties from Özisik [28] calculated at the mean temperature $T_{\mathrm{m}} = T_0 + T_{\mathrm{f}}/2 = 482.5$ °C, $\rho = 838.3$ $\mathrm{kg/m^3}$, $\mu = 2.43 \times 10^{-4}$ $\mathrm{kg/(m\ s)}$, $k = 66.88$

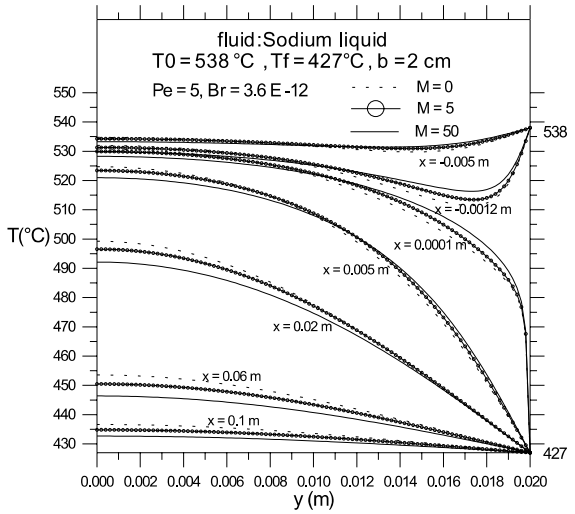

Fig. 10. Radial temperature profiles for sodium liquid for $Pe = 5$, for various axial distances x and Hartmann numbers M.

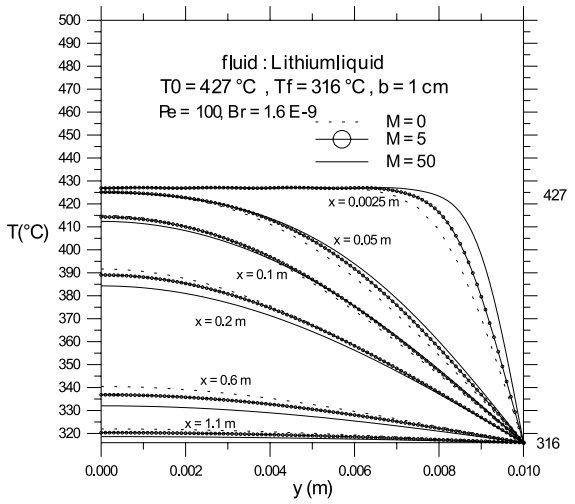

Fig. 11. Radial temperature profiles for lithium liquid for $Pe = 100$, for various axial distances x and Hartmann numbers M.

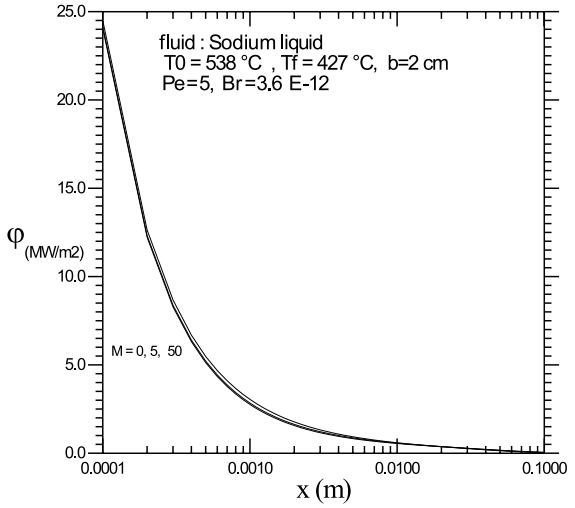

Fig. 12. The local heat flux in the entrance region with various values of Hartmann number in the case of sodium liquid for $Pe = 5$.

W/(m °C), $\alpha = 63.1 \times 10^{-6}$ m^2/s, $Pr = 0.0046$, $Re = 1087$ (where Re is the Reynolds number), $b = 2$ cm with $Pe = Re\,Pr = 5$ and $Br = 3.6 \times 10^{-12}$ and for lithium liquid at $T_0 = 427$ °C, and $T_f = 316$ °C, $\rho = 493.9$ kg/m^3, $\mu = 4.2 \times 10^{-4}$ kg/(m s), $k = 40.66$ W/(m °C), $\alpha = 19.48 \times 10^{-6}$ m^2/s, $Pr = 0.04375$, $Re = 2286$, $b = 1$ cm with $Pe = 100$ and $Br = 1.6 \times 10^{-9}$. For liquid metals the Brinkman number is very small, so the effect of heating by Joule and viscous dissipation can be neglected and the heat transfer is controlled only by convection and conduction.

The thermal entrance lengths Xt defined as the axial position at which the temperature at the center line reaches its fully developed value (the thermally developed temperature) as $T - T_f/T_0 - T_f = 1\%$, is of order of $Xt \sim 0.15$ m for sodium liquid and $Xt \sim 1.5$ m for lithium liquid for $M = 5$ (Figs. 10 and 11). We can deduct approximately the law's variation of the thermal entrance lengths Xt. It can be shown that Xt is approximately of the order of: $Xt \sim 1.5bPe$ for $M = 5$, $Xt \sim 1.7bPe$ for $M = 0$ and $Xt \sim 1.3bPe$ for $M = 50$.

Figs. 10 and 11 show that Xt decreases as the magnetic field increases. We can notice particularly in Fig. 11 that the effect of axial heat conduction decreases for $Pe = 100$ and the temperature tends to uniform temperature profile near the entrance section except near the wall where we have a thermal boundary layer with a strong temperature gradient. Fig. 12 shows that the local heat flux does not appear to be significantly affected by the magnetic field in the thermally

developed region and the increase of the local Nusselt number with M (see Fig. 5) is due principally to the decreasing of the bulk temperature with increasing of the magnetic field.

5. Conclusion

The problem of laminar MHD flow in the thermal entrance region, including viscous dissipation, Joule heating, various operational modes of the channel and axial heat conduction with Dirichlet wall boundary conditions is analyzed by considering infinite axial domain. Several conclusions have been obtained.

1. The solution presented here has the advantage over the numerical method by efficiently solving singularity. This is clearly demonstrated by the results obtained in the neighborhood of $\xi = 0$ (Figs. 2 and 3 and 5–9). Indeed, the singularity causes a problem (Gibbs oscillation) for numerical modelers when evaluating the axial temperature derivative near $\xi = 0$ [14]. The nicety of the solution comes from the fact that variational method no longer has to be used [18] for determination of the expansion coefficients. The validity of the analytical solution is verified by the results of Table 1, which shows that the eigenvalues are in agreement with those reported in [22].

2. In the absence of viscous dissipation and Joule heating, $Br = 0$; the results show that the Hartmann effect produces a decreasing of the bulk temperature.

3. For thermally developing flow when $Br \neq 0$, it is shown that viscous dissipation and Joule heating play a significantly different role in the heat transfer, depending on the electrical condition of the walls. For insulating walls ($\chi = -1$), it was found that the characteristic curves for local Nu do not decrease monotonically along the axial distance particularly for the thermally developed region and Nu increases with M. For perfectly conducting walls ($\chi = 0$), results show that Nu decreases near the entrance section with increasing M and the trend is opposite in the thermally developed region where Nu is little sensitive to M. Unlike the previous study [22], it was found that $Nu_{\text{as.}}$ for $\chi = -1$, is larger than $Nu_{\text{as.}}$ for $\chi = 0$ for fixed and large values of the Hartmann number.

Appendix A

Equating the coefficients of the same power on q^{4p+n}, q^{4p+n+2}, z^{2p}, z^{2p+1}, $\mathrm{ch}(\sqrt{a} \pm 2(n-k))$ and $\mathrm{sh}(\sqrt{a} \pm 2(n-k))$ to zero we get the following recurrence relations for the coefficients $A^n_{\pm(n-k),4p+n}$ and $C^n_{\pm(n-k),4p+n}$:

$$A^1_{1,4+1} + A^1_{-1,4p+1} = -2(2p+1)\sqrt{a}C^0_{0,4p} \quad \text{for } p \geqslant 0, \tag{A.1}$$

$$A^2_{1,4p+2} + A^2_{-1,4p+2} = -2(2p+1)\sqrt{a}C^1_{0,4p+1} \quad \text{for } p \geqslant 0, \tag{A.2}$$

$$A^n_{1,4p+n} + A^n_{-1,4p+n} + A^{n-3}_{0,4p+n+1}(2p+2)(2p+1) = -2(2p+1)\sqrt{a}C^{n-1}_{0,4p+n-1} \quad \text{for } p \geqslant 0 \text{ and } n \geqslant 3, \tag{A.3}$$

$$C^1_{1,4p+1} + C^1_{-1,4p+1} = -(4p+4)\sqrt{a}A^0_{0,4p+4} \quad \text{for } p \geqslant 0, \tag{A.4}$$

$$C^2_{1,4p+2} + C^2_{-1,4p+2} = -(4p+4)\sqrt{a}A^1_{0,4p+5} \quad \text{for } p \geqslant 0, \tag{A.5}$$

$$C^n_{1,4p+n} + C^n_{-1,4p+n} + C^{n-3}_{0,4p+n+1}(2p+2)(2p+3) = -(4p+4)\sqrt{a}A^{n-1}_{0,4p+n+3} \quad \text{for } p \geqslant 0 \text{ and } n \geqslant 3, \tag{A.6}$$

$$A^n_{\pm k,4p+n} = 0 \quad \text{for } k \geqslant n+1 \ (p \geqslant 0 \text{ and } n \geqslant 1), \tag{A.7}$$

$$A^n_{\pm n,4p+n}\left[(\sqrt{a} \pm 2n)^2 - a\right] + A^{n-1}_{\pm(n-1),4p+n-1} = 0 \quad \text{for } p \geqslant 0 \text{ and } n \geqslant 1, \tag{A.8}$$

$$A^n_{\pm(n-1),4p+n}\left[(\sqrt{a} \pm 2(n-1))^2 - a\right] + A^{n-1}_{\pm(n-2),4p+n-1} = 0 \quad \text{for } p \geqslant 0 \text{ and } n \geqslant 2, \tag{A.9}$$

$$\begin{aligned} &A^n_{\pm(n-2),4p+n}\left[(\sqrt{a} \pm 2(n-2))^2 - a\right] + A^{n-1}_{\pm(n-3),4p+n-1} \\ &\quad + A^{n-1}_{\pm(n-1),4p+n-1} + 2(2p+1)\left[\sqrt{a} \pm 2(n-2)\right]C^{n-2}_{\pm(n-2),4p+n-2} = 0 \quad \text{for } p \geqslant 0 \text{ and } n \geqslant 3, \end{aligned} \tag{A.10}$$

$$\begin{aligned} &A^n_{\pm(n-3),4p+n}\left[(\sqrt{a} \pm 2(n-3))^2 - a\right] + A^{n-1}_{\pm(n-4),4p+n-1} + A^{n-1}_{\pm(n-2),4p+n-1} \\ &\quad + 2(2p+1)\left[\sqrt{a} \pm 2(n-3)\right]C^{n-2}_{\pm(n-3),4p+n-2} = 0 \quad \text{for } p \geqslant 0 \text{ and } n \geqslant 4, \end{aligned} \tag{A.11}$$

$$A^n_{\pm(n-k),4p+n}\left[(\sqrt{a}\pm 2(n-k))^2-a\right]+A^{n-1}_{\pm(n-k-1),4p+n-1}+A^{n-1}_{\pm(n-k+1),4p+n-1}+(2p+2)(2p+1)A^{n-4}_{\pm(n-k),4p+n}$$
$$+2(2p+1)\left[\sqrt{a}\pm 2(n-k)\right]C^{n-2}_{\pm(n-k),4p+n-2}=0 \quad \text{for } p\geqslant 0 \text{ and } 4\leqslant k\leqslant n-1, \tag{A.12}$$

$$C^n_{\pm k,4p+n}=0 \quad \text{for } k\geqslant n+1 \ (p\geqslant 0 \text{ and } n\geqslant 1), \tag{A.13}$$

$$C^n_{\pm n,4p+n}\left[(\sqrt{a}\pm 2n)^2-a\right]+C^{n-1}_{\pm(n-1),4p+n-1}=0 \quad \text{for } p\geqslant 0 \text{ and } n\geqslant 1, \tag{A.14}$$

$$C^n_{\pm(n-1),4p+n}\left[(\sqrt{a}\pm 2(n-1))^2-a\right]+C^{n-1}_{\pm(n-2),4p+n-1}=0 \quad \text{for } p\geqslant 0 \text{ and } n\geqslant 2, \tag{A.15}$$

$$C^n_{\pm(n-2),4p+n}\left[(\sqrt{a}\pm 2(n-2))^2-a\right]+C^{n-1}_{\pm(n-3),4p+n-1}$$
$$+C^{n-1}_{\pm(n-1),4p+n-1}+(4p+4)\left[\sqrt{a}\pm 2(n-2)\right]A^{n-2}_{\pm(n-2),4p+n+2}=0 \quad \text{for } p\geqslant 0 \text{ and } n\geqslant 3, \tag{A.16}$$

$$C^n_{\pm(n-3),4p+n}\left[(\sqrt{a}\pm 2(n-3))^2-a\right]+C^{n-1}_{\pm(n-4),4p+n-1}$$
$$+C^{n-1}_{\pm(n-2),4p+n-1}+(4p+4)\left[\sqrt{a}\pm 2(n-3)\right]A^{n-2}_{\pm(n-3),4p+n+2}=0 \quad \text{for } p\geqslant 0 \text{ and } n\geqslant 4, \tag{A.17}$$

$$C^n_{\pm(n-k),4p+n}\left[(\sqrt{a}\pm 2(n-k))^2-a\right]+C^{n-1}_{\pm(n-k-1),4p+n-1}+C^{n-1}_{\pm(n-k+1),4p+n-1}$$
$$+(2p+3)(2p+2)C^{n-4}_{\pm(n-k),4p+n}+(4p+4)\left[\sqrt{a}\pm 2(n-k)\right]A^{n-2}_{\pm(n-k),4p+n+2}=0 \quad \text{for } p\geqslant 0 \text{ and } 4\leqslant k\leqslant n-1. \tag{A.18}$$

Appendix B. Expressions of the coefficients $A^n_{m,4p+n}$, $C^n_{m,4p+n}$

The coefficients $A^n_{\pm(n-k),4p+n}$, $C^n_{\pm(n-k),4p+n}$ are calculated in terms of the arbitrary coefficient $A^0_{0,0}$. In order to normalize Mathieu's function, we take arbitrarily $h_n(0)=1$, this condition fixed $A^0_{0,0}$ and from the recurrence relations given in Appendix A we obtain:

$$\begin{aligned} A^0_{0,0} &= 1,\\ A^1_{0,1} &= -\frac{A^0_{0,0}}{2(a-1)},\\ A^n_{0,n} &= -\sum_{\substack{k=-n\\(k\neq 0)}}^{+n} A^n_{k,n} \quad \text{for } n\geqslant 2. \end{aligned} \tag{B.1}$$

$$\begin{aligned} A^0_{0,4p} &= \alpha(a,p)A^0_{0,0},\\ A^1_{0,4p+1} &= \alpha(a,p)A^1_{0,1},\\ A^2_{0,4p+2} &= \alpha(a,p)A^2_{0,2}+\beta(a,p)A^0_{0,0},\\ A^3_{0,4p+3} &= \alpha(a,p)A^3_{0,3}+\beta(a,p)A^1_{0,1}, \end{aligned} \tag{B.2}$$

where

$$\alpha(a,p)=\frac{\sqrt{\pi}}{64^p a^p(a-1)^{2p}\Gamma(p+1)\Gamma(p+\frac{1}{2})}A^0_{0,0},$$

and

$$\beta(a,p)=\frac{(15a^2-35a+8)\sqrt{\pi}}{8.64^p a^{p+1}(a-1)^{2p+2}(a-4)\Gamma(p)\Gamma(p+\frac{1}{2})}A^0_{0,0}.$$

$$
\begin{aligned}
C^0_{0,4p} &= -\frac{A^0_{0,4p}}{4(2p+1)\sqrt{a}(a-1)},\\
C^1_{0,4p+1} &= -\frac{A^1_{0,4p+1}}{4(2p+1)\sqrt{a}(a-1)},\\
C^2_{0,4p+2} &= -\frac{A^2_{0,4p+2}}{4(2p+1)\sqrt{a}(a-1)} - \frac{(15a^2-35a+8)A^0_{0,4p}}{64(2p+1)a\sqrt{a}(a-1)^3(a-4)},\\
C^3_{0,4p+3} &= -\frac{A^3_{0,4p+3}}{4(2p+1)\sqrt{a}(a-1)} - \frac{(15a^2-35a+8)A^1_{0,4p+1}}{64(2p+1)a\sqrt{a}(a-1)^3(a-4)},
\end{aligned}
\tag{B.3}
$$

$$A^n_{n,4p+n} = U_n A^0_{0,4p} \quad \text{for } n \geqslant 1 \text{ and } p \geqslant 0, \tag{B.4}$$

$$A^n_{n-1,4p+n} = U_{n-1} A^1_{0,4p+1} \quad \text{for } n \geqslant 2 \text{ and } p \geqslant 0, \tag{B.5}$$

$$A^n_{n-2,4p+n} = U_{n-2}\left\{ A^2_{0,4p+2} + \frac{A^0_{0,4p}}{16}\sum_{j=1}^{n-2} S_1(j) - \frac{(2p+1)}{2} C^0_{0,4p}\sum_{j=1}^{n-2} S_2(j)\right\} \quad \text{for } n \geqslant 3 \text{ and } p \geqslant 0, \tag{B.6}$$

$$A^n_{n-3,4p+n} = U_{n-3}\left\{ A^3_{0,4p+3} + \frac{A^1_{0,4p+1}}{16}\sum_{j=1}^{n-3} S_1(j) - \frac{(2p+1)}{2} C^1_{0,4p+1}\sum_{j=1}^{n-3} S_2(j)\right\} \quad \text{for } n \geqslant 4 \text{ and } p \geqslant 0, \tag{B.7}$$

$$A^n_{-(n-k),4p+n} = \overline{A^n_{n-k,4p+n}},\quad C^n_{-(n-k),4p+n} = -\overline{C^n_{n-k,4p+n}},$$

where $\overline{(\,)}$ denotes the complex conjugate.

With

$$U_n = \frac{(-1)^n \Gamma(1+\sqrt{a})}{4^n \Gamma(n+1)\Gamma(n+1+\sqrt{a})},$$

$$S_1(j) = \frac{1}{j(j+1)(j+\sqrt{a})(j+1+\sqrt{a})},$$

$$S_2(j) = \frac{1}{j} + \frac{1}{j+\sqrt{a}},$$

$$C^n_{n,4p+n} = U_n C^0_{0,4p} \quad \text{for } n \geqslant 1 \text{ and } p \geqslant 0, \tag{B.8}$$

$$C^n_{n-1,4p+n} = U_{n-1} C^1_{0,4p+1} \quad \text{for } n \geqslant 2 \text{ and } p \geqslant 0, \tag{B.9}$$

$$C^n_{n-2,4p+n} = U_{n-2}\left\{ C^2_{0,4p+2} + \frac{C^0_{0,4p}}{16}\sum_{j=1}^{n-2} S_1(j) - (p+1)A^0_{0,4p+4}\sum_{j=1}^{n-2} S_2(j)\right\} \quad \text{for } n \geqslant 3 \text{ and } p \geqslant 0, \tag{B.10}$$

$$C^n_{n-3,4p+n} = U_{n-3}\left\{ C^3_{0,4p+3} + \frac{C^1_{0,4p+1}}{16}\sum_{j=1}^{n-3} S_1(j) - (p+1)A^1_{0,4p+5}\sum_{j=1}^{n-3} S_2(j)\right\} \quad \text{for } n \geqslant 4 \text{ and } p \geqslant 0. \tag{B.11}$$

For higher-order $k \geqslant 4$, the explicit general forms of coefficients $A^n_{n-k,4p+n}$, $C^n_{n-k,4p+n}$ are increasingly more difficult to obtain. However, for $k \geqslant 4$ these coefficients can be determined by using recurrence relations (A.12) and (A.17).

References

[1] C.J. Hsu, An exact analysis of low peclet number thermal entry region heat transfer in transversely non uniform velocity fields, A.I.C.H.E. J. 17 (1971) 732–740.

[2] C.E. Smith, M. Faghri, J.R. Welty, On the determination of temperature distribution laminar pipe flow with a step change in wall heat flux, J. Heat Transfer C 97 (1975) 137–179.

[3] J.C. Pirkle, V.G. Sigillito, A variational approach to low Peclet number heat transfer in laminar flow, J. Comput. Phys. 9 (1972) 207–221.

[4] A.S. Jones, Extensions to the solution of the Graetz problem, Int. J. Heat Mass Transfer 14 (1971) 619–623.

[5] A. Acrivos, The extended Graetz problem at low Peclet number, Appl. Sci. Res. 36 (1980) 35–40.

[6] Y. Bayazitoglu, M.N. Özisik, On the solution of Graetz type problems with axial conduction, Int. J. Heat Mass Transfer 23 (1980) 1399–1402.
[7] C. Laohakul, C.Y. Chan, K.Y. Look, C.W. Tan, On approximate solutions of the Graetz problem with axial conduction, Int. J. Heat Mass Transfer 28 (1985) 541–545.
[8] E. Papoutsakis, D. Ramkrishna, H.C. Lim, The extended Graetz problem with Dirichlet wall boundary conditions, Appl. Sci. Res. 36 (1980) 13–34.
[9] T. Min, J.Y. Yoo, Laminar convective heat transfer of a Bingham plastic in a circular pipe with uniform wall heat flux: the Graetz problem extended, J. Heat Transfer 121 (1999) 556–563.
[10] J. Lahjomri, A. Oubarra, Analytical solution of the Graetz problem with axial conduction, J. Heat Transfer 121 (1999) 1078–1083.
[11] D.K. Hennecke, Heat transfer by Hagen–Poiseuille flow in the thermal development region with axial conduction, Wärme-Stoffübetragung Bd. 1 (1968) 177–184.
[12] F.H. Verhoff, D.P. Fisher, A numerical solution of the Graetz problem with axial conduction, J. Heat Transfer 95 (1973) 132–134.
[13] M.L. Michelsen, J. Villadsen, The Graetz problem with axial heat conduction, Int. J. Heat Mass Transfer 17 (1974) 1391–1402.
[14] H.C. Ku, D. Hatziavramidis, Chebyshev expansion methods for the solution of the extended Graetz problem, J. Comput. Phys. 56 (1984) 495–512.
[15] C.T. Liou, F.S. Wang, Solution to the extended Graetz problem for a power-model fluid with viscous dissipation and different entrance boundary conditions, Numer. Heat Transfer, Part A 17 (1990) 91–108.
[16] C.T. Liou, F.S. Wang, A computation for the boundary value problem of a double tube heat exchanger, Numer. Heat Transfer, Part A 17 (1990) 109–125.
[17] L. Graetz, Über die wärmeleitungsfähigkeit von flüssigkeiten, Ann. Phys. Chem. 25 (1885) 337–357.
[18] S.D. Nigam, S.N. Singh, Heat transfer by laminar flow between parallel plates under the action of transverse magnetic field, Quart. J. Mech. Appl. Math. XIII (Pt. 1) (1960) 85–97.
[19] I. Michiyoshi, R. Matsumato, Heat transfer by Hartmann's flow in thermal entrance region, Int. J. Heat Mass Transfer 7 (1964) 101–111.
[20] C.L. Hwang, P.J. Knieper, L.T. Fan, Heat transfer to MHD flow in the entrance of a flat duct, Int. J. Heat Mass Transfer 9 (1966) 773–789.
[21] V. Javeri, Magnetohydrodynamic channel flow heat transfer for temperature boundary condition of the third kind, Int. J. Heat Mass Transfer 20 (1977) 543–547.
[22] R.C. LeCroy, A.H. Eraslan, The solution of temperature development in the entrance region of an MHD channel by the B.G. Galerkin method, J. Heat Transfer C 91 (1969) 212–220.
[23] R.S. Wu, K.C. Cheng, Thermal entrance region heat transfer for MHD laminar flow in parallel-plate channels with unequal wall temperatures, Wärme-und Stoffübertragung 9 (1976) 273–280.
[24] M. Abramowitz, I.A. Stegun, Handbook of Mathematical Functions, NBS Applied Mathematics Series 55, 1972, p. 722 (Chapter 20).
[25] J.R. Sellars, M. Tribus, J.S. Klein, Heat transfer to laminar flow in a round tube or flat conduit – the Graetz problem extended, Trans. Am. Soc. Mech. Engrs. 78 (1956) 441–448.
[26] C. Housiadas, F.E. Larrodé, Y. Drosinos, Numerical evaluation of the Graetz series, Int. J. Heat Mass Transfer 42 (1999) 3013–3017.
[27] A. Bejan, Convection Heat Transfer, second ed., Wiley, New York, 1995.
[28] M.N. Özisik, A Heat Transfer. A Basic Approach, Tome 4, McGraw-Hill, New York, p. 744.